



LAWRENCE
LIVERMORE
NATIONAL
LABORATORY

Numerical Simulations of Thermobaric Explosions

Allen L. Kuhl, John B. Bell, Vincent E. Beckner,
Boris Khasainov

May 30, 2007

37th International Annual Conference Energetic Materials
Characterisation and Performance of Advanced Systems
Karlsruhe, Germany
June 26, 2007 through June 29, 2007

This document was prepared as an account of work sponsored by an agency of the United States Government. Neither the United States Government nor the University of California nor any of their employees, makes any warranty, express or implied, or assumes any legal liability or responsibility for the accuracy, completeness, or usefulness of any information, apparatus, product, or process disclosed, or represents that its use would not infringe privately owned rights. Reference herein to any specific commercial product, process, or service by trade name, trademark, manufacturer, or otherwise, does not necessarily constitute or imply its endorsement, recommendation, or favoring by the United States Government or the University of California. The views and opinions of authors expressed herein do not necessarily state or reflect those of the United States Government or the University of California, and shall not be used for advertising or product endorsement purposes.

NUMERICAL SIMULATIONS OF THERMOBARIC EXPLOSIONS

Allen L. Kuhl¹, John B. Bell², Vincent E. Beckner² & Boris Khasainov³

¹ Lawrence Livermore National Laboratory, P.O. Box 808, Livermore, CA 94551 USA

² Lawrence Berkeley National Lab., 1 Cyclotron Rd, Berkeley, CA, 94720 USA

³ Laboratoire de Combustion et Détonique, UPR 9028 CNRS, 86961 Futuroscope, France

ABSTRACT

A Model of the energy evolution in thermobaric explosions is presented. It is based on the two-phase formulation: conservation laws for the gas and particle phases along with inter-phase interaction terms. It incorporates a Combustion Model based on the mass conservation laws for fuel, air and products; source/sink terms are treated in the fast-chemistry limit appropriate for such gasdynamic fields. The Model takes into account both the afterburning of the detonation products of the booster with air, and the combustion of the fuel (Al or TNT detonation products) with air. Numerical simulations were performed for 1.5-g thermobaric explosions in five different chambers (volumes ranging from 6.6 to 40 liters and length-to-diameter ratios from 1 to 12.5). Computed pressure waveforms were very similar to measured waveforms in all cases—thereby proving that the Model correctly predicts the energy evolution in such explosions. The computed global fuel consumption $\mu(t)$ behaved as an exponential life function. Its derivative $\dot{\mu}(t)$ represents the global rate of fuel consumption. It depends on the rate of turbulent mixing which controls the rate of energy release in thermobaric explosions.

INTRODUCTION

We model experiments of Shock-Dispersed-Fuel (SDF) explosions in various calorimetric chambers. The SDF charge concept was presented at previous ICT Conferences by Neuwald [1, 2, 3]; results from parametric studies are summarized in a companion paper at this Conference [4]. We have shown SDF charge is the most efficient design to maximize the thermobaric effect [5]. Construction of the charge will be shown in a later figure. It consisted of a 0.5-g spherical PETN booster and 1-g of fuel (either flake Aluminum or a spherical shell of TNT). Detonation of the booster disperses the fuel and heats it; when it mixes with air it releases the heat of combustion by a non-premixed turbulent combustion process. This heats the explosion cloud to combustion-like temperatures (2,000-4,000 K)—thereby creating the thermobaric effect.

Presented here is a two-phase model of the explosion/combustion process. It is based on gas-dynamic conservation laws for the gas phase, dilute continuum conservation laws for the particle phase, and inter-phase interaction terms, as formulated by Nigmatulin [6]. Afterburning of the booster detonation products with air, and combustion of the fuel with air are both taken into account in the combustion model. Thermodynamic properties of the components are described in a companion paper [7]. It is worthy to note that compared to our former model [8], we not only simplified the equation of state (EOS), but also extended the number of components. In addition, these Model equations are integrated with our Adaptive Mesh Refinement (AMR) code to describe the evolution of mixing and combustion in thermobaric explosions.

MODEL

Conservation Laws

The model is based on the Eulerian multi-phase conservation laws for a dilute heterogeneous continuum, as formulated by Nigmatulin [6]. We model the evolution of the gas phase combustion fields in the limit of large Reynolds and Peclet numbers, where effects of molecular diffusion and heat conduction are negligible. The flow field is governed by the gas-dynamic conservation laws:

$$\text{Mass:} \quad \partial_t \rho + \nabla \cdot (\rho \mathbf{u}) = \dot{\sigma}_s \quad (1)$$

$$\text{Momentum:} \quad \partial_t \rho \mathbf{u} + \nabla \cdot (\rho \mathbf{u} \mathbf{u} + p) = \dot{\sigma}_s \mathbf{v} - \dot{f}_s \quad (2)$$

$$\text{Energy:} \quad \partial_t \rho E + \nabla \cdot (\rho \mathbf{u} E + p \mathbf{u}) = -\dot{q}_s + \dot{\sigma}_s E_s - \dot{f}_s \cdot \mathbf{v} \quad (3)$$

where ρ, p, u represent the gas density, pressure and specific internal energy, \mathbf{u} is the gas velocity vector, and $E \equiv u + \mathbf{u} \cdot \mathbf{u}/2$ denotes the total energy of the gas phase. Source terms on the right hand side take into account: mass addition to gas phase due to particle burning ($\dot{\sigma}_s$), particle drag (\dot{f}_s), and heat losses (\dot{q}_s).

We treat the particle phase as a Eulerian continuum field. We consider the dilute limit, devoid of particle-particle interactions, so that the pressure and sound speed of the particle phase are zero. We model the evolution of particle phase mass, momentum and energy fields by the conservation laws of continuum mechanics for heterogeneous media:

$$\text{Mass:} \quad \partial_t \sigma + \nabla \cdot \sigma \mathbf{v} = -\dot{\sigma}_s \quad (4)$$

$$\text{Momentum:} \quad \partial_t \sigma \mathbf{v} + \nabla \cdot \sigma \mathbf{v} \mathbf{v} = -\dot{\sigma}_s \mathbf{v} + \dot{f}_s \quad (5)$$

$$\text{Energy:} \quad \partial_t \sigma E_s + \nabla \cdot \sigma E_s \mathbf{v} = \dot{q}_s - \dot{\sigma}_s E_s + \dot{f}_s \cdot \mathbf{v} \quad (6)$$

$$\text{Particles:} \quad \partial_t n_s + \nabla \cdot n_s \mathbf{v} = 0 \quad (7)$$

where σ and \mathbf{v} represent the particle-phase density and velocity, n is the number of particles, and $E_s \equiv C_s T_s + \mathbf{v} \cdot \mathbf{v}/2$ denotes the total energy of the particle phase.

Interactions

The inter-phase interaction terms for mass, momentum, heat and particle burning law take the form as described by Khasainov et al. [8]:

$$\text{Mass Exchange:} \quad \dot{\sigma}_s = \begin{cases} 0 & T_s < T_{ign} \\ -3\sigma(1 + 0.276\sqrt{\text{Re}_s})/t_s & T_s \geq T_{ign} \end{cases} : \quad (8)$$

$$\text{Momentum Exchange:} \quad \dot{f}_s = \frac{3}{4} \frac{\rho}{\rho_s} \frac{\sigma}{d_s} C_D (\mathbf{u} - \mathbf{v}) |\mathbf{u} - \mathbf{v}| \quad (9)$$

$$\text{where } C_D = 24/\text{Re}_s + 4.4/\sqrt{\text{Re}_s} + 0.42 \text{ and } \text{Re}_s = \rho d_s |\mathbf{u} - \mathbf{v}|/\mu \quad (10)$$

$$\text{Heat Exchange:} \quad \dot{q}_s = \frac{6\sigma}{\rho_s d_s} \left[\frac{Nu\lambda(T - T_s)}{d_s} + \varepsilon\sigma_{\text{Boltz}}(T^4 - T_s^4) \right] \quad (11)$$

$$\text{where } Nu = 2 + 0.6\text{Pr}\sqrt{\text{Re}_s} \quad (12)$$

$$\text{Burning Law [9]:} \quad t_s = Kd_{s0}^n / \phi^{0.9} \quad (13)$$

Combustion

We consider three fuels: PETN detonation products (F_1), TNT detonation products (F_2), and Aluminum (F_3), along with their corresponding combustion products: PETN-air (P_1), TNT-air (P_2) and Al-air (P_3). We consider the global combustion of fuel F_k with air (A) producing equilibrium combustion products P_k :



The mass fractions Y_k of the components are governed by the following conservation laws:

$$\text{Fuel-}k: \quad \partial_t \rho Y_{Fk} + \nabla \cdot \rho Y_{Fk} \mathbf{u} = -\dot{s}_k + \delta_{k3} \dot{\sigma}_k \quad (15)$$

$$\text{Air:} \quad \partial_t \rho Y_A + \nabla \cdot \rho Y_A \mathbf{u} = -\sum_k \alpha_k \dot{s}_k \quad (16)$$

$$\text{Products-}k: \quad \partial_t \rho Y_{Pk} + \nabla \cdot \rho Y_{Pk} \mathbf{u} = \sum_k (1 + \alpha_k) \dot{s}_k \quad (17)$$

Fuel and air are consumed in stoichiometric proportions: $\alpha_k = A/F_k$. In the above, \dot{s}_k represents the global kinetics sink term. In this work we use the fast-chemistry limit that is consistent with the inviscid gas-dynamic model (1)-(3), so whenever fuel and air enter a computational cell, they are consumed in one time step. The symbol δ_{k3} represents the Kronecker delta ($\delta_{k3} = 1$ if $k = 3$ and $\delta_{k3} = 0$ if $k \neq 3$) and takes into account the vaporization of Al fuel from the particle phase EQ. (4), which creates a source of Al fuel in the gas phase.

To clarify the notation of (15)-(17), the case with $k=1$ denotes PETN-air afterburning, the case with $k=2$ corresponds to TNT-air afterburning, and the case $k=3$ represents Al-air combustion. In addition, two global combustion processes can also be considered (assuming that the fuels F_k do not react with each other). Combination $k = \{1,2\}$ models the afterburning of PETN and TNT in air from a composite TNT-SDF charge explosion (without Al), while combination $k = \{1,3\}$ models the afterburning of PETN and combustion of Aluminum with air in an Al-SDF charge explosion.

Equations of State

Our code carries the mixture density and specific internal energy, along with the composition in each cell. These are used to calculate the pressure and temperature in a computational cell based on Equations of State (EOS). The thermodynamic states encountered during SDF explosions have been analyzed in a companion paper [7]. Here we summarize only the salient features needed for the numerical modeling.

Figure 1 presents the locus of states in the $u - T$ plane of specific internal energy versus temperature. Indicated there are curves for Reactant components (PETN and TNT detonation products, aluminum and air) and their corresponding equilibrium combustion Products components. In [7] we have shown that these components behave as calorically-perfect gases for $T < 3,500K$. Thus it is appropriate to fit them solely as a function of temperature. Piecewise quadratic functions were used to define the components c :

$$u_c(T) = a_c T^2 + b_c T + c_c \quad (c = A, DP, R, P) \quad (18)$$

The coefficient values a_c, b_c, c_c may be found in the Appendix of [7]. For computational cells containing a mixture of components, the mixture energy also satisfies a quadratic form:

$$u_m(T) = \sum_c Y_c u_c = a_m T_m^2 + b_m T_m + c_m \quad (19)$$

Given the mixture specific internal energy u_m , the mixture temperature can be evaluated by:

$$T_m = [-b_m + \sqrt{b_m^2 - 4a_m(c_m - u_m)}] / 2a_m \quad (20)$$

using mixture coefficients as defined by:

$$a_m = \sum_c Y_c a_c, b_m = \sum_c Y_c b_c, c_m = \sum_c Y_c c_c, R_m = \sum_c Y_c R_c \quad (21)$$

For pure cells, the pressure of a component is calculated from the perfect gas relation $p_c = \rho_c R_c T_c$, or from the JWL function in the detonation products gases [7]. In mixed cells, the pressure is calculated from the mixture temperature by the law of additive pressures [10]:

$$p_m = \sum_c p_c(V_m, T_m) \quad (22)$$

where $p_c(V_m, T_m)$ denotes the pressure that would be exerted by component c if it existed alone at the temperature and volume of the mixture.

Numerical Methods

The governing equations (1)-(7) and (15)-(17) are integrated with high-resolution upwind methods that represent high order generalizations of Godunov's method [11]. The algorithm for gas phase conservation laws is based on an efficient Riemann solver for gas-dynamics first developed by Colella et al. [12,13] and extended to generalized conservation laws by Bell et al. [14] and Colella [15]. The algorithm for the particle phase conservation laws is based on a Riemann solver for two-phase flows as developed by Collins et al. [16]. Source terms are treated with operator splitting methods. Being based on Riemann solvers, information propagates along characteristics at the correct wave speeds, and they incorporate nonlinear wave interactions within the cell during the time step. They include a limiting step that automatically reduces the order of approximation in the neighborhood of discontinuities, while in smooth regions of the flow the scheme is second order in time and space.

These Godunov schemes have been integrated into an adaptive mesh refinement (AMR) algorithm that allows us to focus computational effort in complex regions of the flow such as mixing layers and reaction zones. Our adaptive methods are based on the block-structured AMR algorithms of Berger et al. [17] and Colella [18], and extended to three-dimensional hyperbolic systems by Bell et al. [19]. Cartesian grid methods are used to represent irregular geometries [20]. In this AMR approach, regions to be refined are organized into rectangular patches, with several hundred to several thousand grid-points per patch. One can refine on discontinuities (shocks and contact surfaces), on Richardson error estimates, or for present purposes, on flame surfaces and shocks. Grid patches are assigned to processors based on work-load estimates [21], so the AMR code runs efficiently on massively-parallel computers [22].

AMR is also used to refine turbulent mixing regions; by successive refinements we are able to capture the energy-bearing scales of the turbulence on the computational grid. In this way we are able to compute the effects of turbulent mixing without resorting to turbulence modeling (which is not applicable to this problem). This is consistent with the so-called MILES (Monotone Integrated Large Eddy Simulation) approach of Boris et al. [23].

RESULTS

Blast Wave from a Thermobaric Explosion

Numerical simulations of the explosion of an Al-SDF charge (0.5-g PETN + 1.0-g flake Al) in a 6.6-liter calorimeter were performed. We start by considering the initial blast wave expansion field. For times less than the first shock arrival at the calorimeter wall ($t \sim 80 \mu\text{s}$), this flow field may be approximated as a one-dimensional (1D) spherical problem. The two-phase flow field profiles are presented in Fig. 2. Solid curves denote the gas phase while dashed curves represent the particle phase. Expansion of the charge drives a blast wave into the surrounding atmosphere (Fig. 2a). At breakout, a 40 bar air shock is formed; this decays to a peak pressure of 10 bars as the shock approaches the wall ($R = 12 \text{ cm}$). Pressures near center approach zero due to the over-expansion of the detonation products gases. This creates a backward-facing shock evident at $R \sim 5 \text{ cm}$ which implodes at later times. These pressure waveforms are typical of HE-driven blasts, as was first predicted by Brode in 1958 [24].

Both gas and particle velocity profiles are presented in Fig. 2b. The initial velocity profile of the gas phase peaks at 2,300 m/s. In $5 \mu\text{s}$, this accelerates the particle phase to a peak velocity of 1,000 m/s. By $25 \mu\text{s}$, the velocities of the two phases have equilibrated (green curves), with a peak of about 1,500 m/s. At later times the gas velocity field decays faster than that of the particle phase, so that at $t = 75 \mu\text{s}$ the velocity of the particle phase is greater than that of the gas (1,000 m/s versus 800 m/s, respectively), indicating that the particle phase is now accelerating the gas through drag interactions. In effect, the particle cloud acts as a leaky piston.

The gas and particle density profiles are presented in Fig. 2c. The particle cloud starts with a peak density of $1,000 \text{ kg/m}^3$; at later times it decays to 1 kg/m^3 , which is an order of magnitude smaller than the shocked gas densities. The temperature profiles are depicted in Fig. 2d. The initial gas temperature in the blast wave is about 2,500 K. By $5 \mu\text{s}$, the air has

heated the particle cloud to a temperature of 1,000 K (melting of Al at 933 K is seen at $t < 45 \mu s$). After an induction time of about $35 \mu s$, the Aluminum particles ignite. This Al-air combustion raises the temperature of the particle cloud to 2,500 K, thereby heating the surrounding air. So, at early times the air heats the particles, while at later times the particles heat the air (due to combustion effects).

Reynolds number profiles (based on the slip velocity and particle diameter) are provided in Fig. 2e; typical values are very small ($0.01 < Re < 0.1$)—indicating that gas flow among the particles is in the Stokes flow regime, where $C_D \sim 24/Re$. At such small Reynolds numbers, the drag force is very large ($240 < C_D < 2,400$). This large drag causes the phases to rapidly equilibrate—so that the ensemble mixture behaves, in effect, as a one-velocity fluid. One could call this a velocity-equilibrium sub-model of the governing equations.

Mixing and Combustion in Al-SDF Explosions

Next a 3D simulation of Al-SDF explosion in a 6.6-liter cylindrical calorimeter ($L = 21.0 cm, D = 20.0 cm$) was performed. Figure 3 depicts the combustion products interface just before the blast wave reaches the calorimeter wall ($t = 70 \mu s$). Richtmyer-Meshkov instabilities on the Fuel-Air interface lead to the development of a turbulent mixing layer in a spherical shell in the region near the interface ($t = 70 \mu s$ in Fig. 5). Combustion products are thus formed via a non-premixed turbulent combustion process. By 3 ms, combustion products fill the whole calorimeter volume (Fig. 4). This illustrates that by using adaptive refinement, the simulation can capture the turbulent mixing structures on the computational grid (the so-called MILES approach of Boris [23]).

Figure 5 presents the static over-pressure histories measured at $r = 5 cm$ on the roof of the 6.6-liter calorimeter. Four gauge records at different azimuths from one test are displayed; there is remarkable similitude in the records, considering that the flow is highly turbulent. This implies that the pressure field is dominated by shock/acoustic vibration which conform themselves to the geometry of the chamber. Computed pressure waveforms are compared with the data in the same figure. The waveform from the non-equilibrium model (solution of equations (1)-(7)) agrees very well with the measured waveforms.

The computed fuel history is depicted in Fig. 6. Global fuel consumption is well approximated by the exponential *Life Function* of Oppenheim [25]:

$$\mu(t) = 1.12 - 0.363e^{-0.284t} - 0.939e^{-4.20t} \quad (23)$$

where $[t] = ms$ and $\mu = 0$ at $t = 0$. More than 96% of the Al fuel was consumed during 3ms. Its derivative $\dot{\mu}(t)$ represents the global bulk rate of combustion:

$$\dot{\mu}(t) = - \int_{V_c} \dot{s} dV / M_F \quad (24)$$

Afterburning in TNT-SDF Explosions

Numerical simulations of the explosion of a TNT-SDF charge (0.5-g PETN booster + 1.0-g TNT fuel shown in Fig. 3) were performed for various cylindrical calorimeters: Case A (6.6-liter), Case B (20.2-liter) and Case C (40.5-liter), and 6.3-liter calorimetric tunnels: Case D ($L = 55.5\text{ cm}$, $D = 12\text{ cm}$; $L/D = 4.65$) and Case E ($L = 100\text{ cm}$, $X = Y = 8\text{ cm}$; $L/D = 12.5$). A visualization of the combustion products formed by afterburning of the TNT-SDF charge in air was also presented in Fig. 3; it shows that the combustion products region is turbulent. Static over-pressure waveforms measured in experiments in various chambers (A, B, C, D and E) are presented in Fig. 7. Computed waveforms from the 3D AMR simulations are also presented in Fig. 7; they show remarkable similitude with the experimental waveforms.

SUMMARY AND CONCLUSIONS

A Model of the energy evolution in thermobaric explosions has been presented. It is based on the two-phase formulation: conservation laws for the gas and particle phases along with inter-phase interaction terms. It incorporates a Combustion Model based on the mass conservation laws for fuel, air and products components; source/sink terms are treated in the fast chemistry limit appropriate for such explosion fields. The Model takes into account both the afterburning of the detonation products of the PETN booster with air, and the combustion of the fuel (Al or TNT detonation products) with air. The Model accommodates additional global combustion processes such as the combustion of hydrocarbon clouds in thermobaric explosions. Thus it is a generalization of the combustion models we presented previously. Another very important improvement is that the new EOS is three times faster than our previous table lookup routine [8].

Numerical simulations were performed for thermobaric explosions in five different chambers (volumes ranging from 6.6 to 40 liters, and $1 < L/D < 12.5$). Computed pressure waveforms were very similar to measured waveforms in all cases—thereby proving that the Model correctly predicts the energy evolution in this type of thermobaric explosion.

The computed global fuel consumption $\mu(t)$ behaved as an exponential function. Its derivative $\dot{\mu}(t)$ represents the global rate of combustion (i.e., fuel consumption, integrated

over the chamber volume); it is controlled by the rate of turbulent mixing. Thus, to get the correct rate of energy release in numerical simulations of thermobaric explosions, the code must accurately predict the 3D turbulent velocity field. We do this by capturing the energy-bearing scales of the turbulence on the computational grid via adaptive mesh refinement.

ACKNOWLEDGEMENTS

This work was performed under the auspices of the U. S. Department of Energy by the University of California, Lawrence Livermore National Laboratory under Contract No. W-7405-Eng-48. It was sponsored by the Defense Threat Reduction Agency under IACRO # 06-40731.

REFERENCES

- [1] P. Neuwald, H. Reichenbach & A. L. Kuhl “Shock-Dispersed Fuel Charges—Combustion in Chambers and Tunnels”, *Energetic Materials*, 34th ICT Conf, 13.1-13.14, 2003.
- [2] P. Neuwald, H. Reichenbach & A. L. Kuhl, “Shock-Dispersed Flake Aluminum—Performance in Environments of Different Geometries”, *Energetic Materials*, 36th ICT Conf, 71.1-71.12, 2005.
- [3] P. Neuwald, H. Reichenbach, & A. L. Kuhl, “Combustion of Shock-Dispersed-Flake Aluminum—High-Speed Visualization” *Energetic Materials*, 37th ICT Conference, 116.1 to 116.12, 2006.
- [4] H. Reichenbach, P. Neuwald & A. L. Kuhl “Waveforms Measured in Confined Thermobaric Explosions” *Energetic Materials*, 38th ICT Conference, 2007 (in press).
- [5] A. L. Kuhl, P. Neuwald and H. Reichenbach, “Effectiveness of Combustion of Shock-Dispersed Fuels in Calorimeters of Various Volumes” *Combustion, Explosion & Shock Waves*, **42** (6), pp. 731-734, 2006.
- [6] R. I. Nigmatulin, 1987, **Dynamics of Multi-phase Flows**. Vol 1. Moscow, Nauka, 464 pp
- [7] A. L. Kuhl & B. Khasainov “Quadratic Model of Thermodynamic States in SDF Explosions”, *Energetic Materials*, 38th ICT Conference, 2007 (in press).
- [8] B. Khasainov, A. L. Kuhl, S. Victorov & P. Neuwald “Model of Non-Premixed Combustion of Al-Air Mixtures” *14th APS Meeting on Shock Compression Condensed in Matter*, AIP Proceedings 845, part 1, pp. 449-452, 2005
- [9] W. Ingnoli *Etude de la formation et de la propagation des détonations dans des suspensions de particules d'aluminium en atmosphère oxydante ou réactive*. Thèse d'Université de Poitiers, France, 1999.
- [10] J. B. Jones & G. A. Hawkins **Engineering Thermodynamics: An Introductory Textbook**, Wiley, New York, p. 405, 1960.
- [11] B. van Leer, “Towards the Ultimate Conservative Difference Scheme V: a Second-order Sequel to Godunov's Methods”, *J Comp. Phys.*, 32:101-136, 1979.
- [12] P. Colella & H. Glaz, “Efficient Solution Algorithms for the Riemann Problem for Real Gases”, *J Comp. Phys.*, **59**, pp. 264-289, 1985.
- [13] P. Colella & P. R. Woodward, “The Piecewise Parabolic Method (PPM) for Gas-dynamical Simulations”, *J Comp. Phys.*, 54:174-201, 1984.
- [14] J. B. Bell, P. Colella, & J. A. Trangenstein “Higher Order Godunov Methods for General Systems of Hyperbolic Conservation Laws” *J Comp. Phys.*, 92(2):362-397, 1989.
- [15] P. Colella, “Multidimensional Upwind Methods for Hyperbolic Conservation Laws”, *J Comp. Phys.*, 87:171-200, 1990.
- [16] P. Collins, R. E. Ferguson, K. Chien, A. L. Kuhl, J. Krispin & H. M. Glaz, “Simulation of Shock-Induced Dusty Gas Flows Using Various Models”, **AIAA 94-2309**, *AIAA Fluid Dynamics Conference*, 1994.

- [17] M. J. Berger & J. Olinger, “Adaptive Mesh Refinement for Hyperbolic Partial Differential Equations”, *J Comp. Phys.*, **53**: 484-512, 1984.
- [18] M. J. Berger & P. Colella, “Local Adaptive Mesh Refinement for Shock Hydrodynamics”, *J Comp. Phys.*, **82** (1): 64-84, 1989.
- [19] J. Bell, M. Berger, J. Saltzman, & M. Welcome, “A Three-Dimensional Adaptive Mesh Refinement for Hyperbolic Conservation Laws”, *SIAM J. Sci. Statist. Comput.*, **15**(1):127-138, 1994.
- [20] R. B. Pember, J. B. Bell, P. Colella, W.Y. Crutchfield, & M. L. Welcome “An Adaptive Cartesian Grid Method for Unsteady Compressible Flow in Complex Geometries”, *J Comp. Phys.* 120 (2): 278-304, 1995.
- [21] W. Y. Crutchfield & M. L. Welcome, “Object-oriented Implementation of Adaptive Mesh Refinement Algorithms”, *Scientific Programming*, 2:145-156, 1993.
- [22] C. A. Rendleman, V. E. Beckner, M. Lijewski, W. Y. Crutchfield & J. B. Bell, “Parallelization of Structured, Hierarchical Adaptive Mesh Refinement Algorithms”, *Computing and Visualization in Science*, Vol. 3, 2000.
- [23] J. Boris, F. Grinstein, E. Oran, & R. Kolbe “New Insights into Large Eddy Simulation”. *Fluid Dynamics Research*, **10**, 1992.
- [24] H. L. Brode “Blast Wave from a Spherical Charge”, *Phys Fluids*, 2(2), p 217-229, 1959.
- [25] A. K. Oppenheim, *Dynamics of Combustion Systems*, Springer, Berlin, 359 pp., 2006

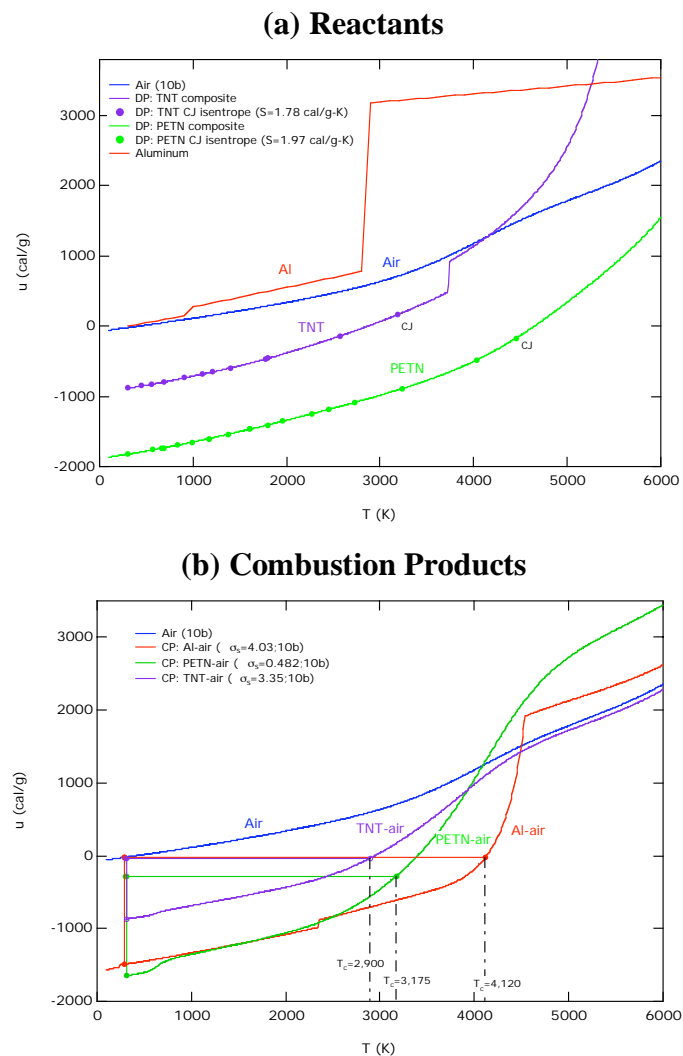


Figure 1. Loci of states for SDF explosions, including components (TNT, PETN and Aluminum) and their corresponding Combustion Products with air [7].

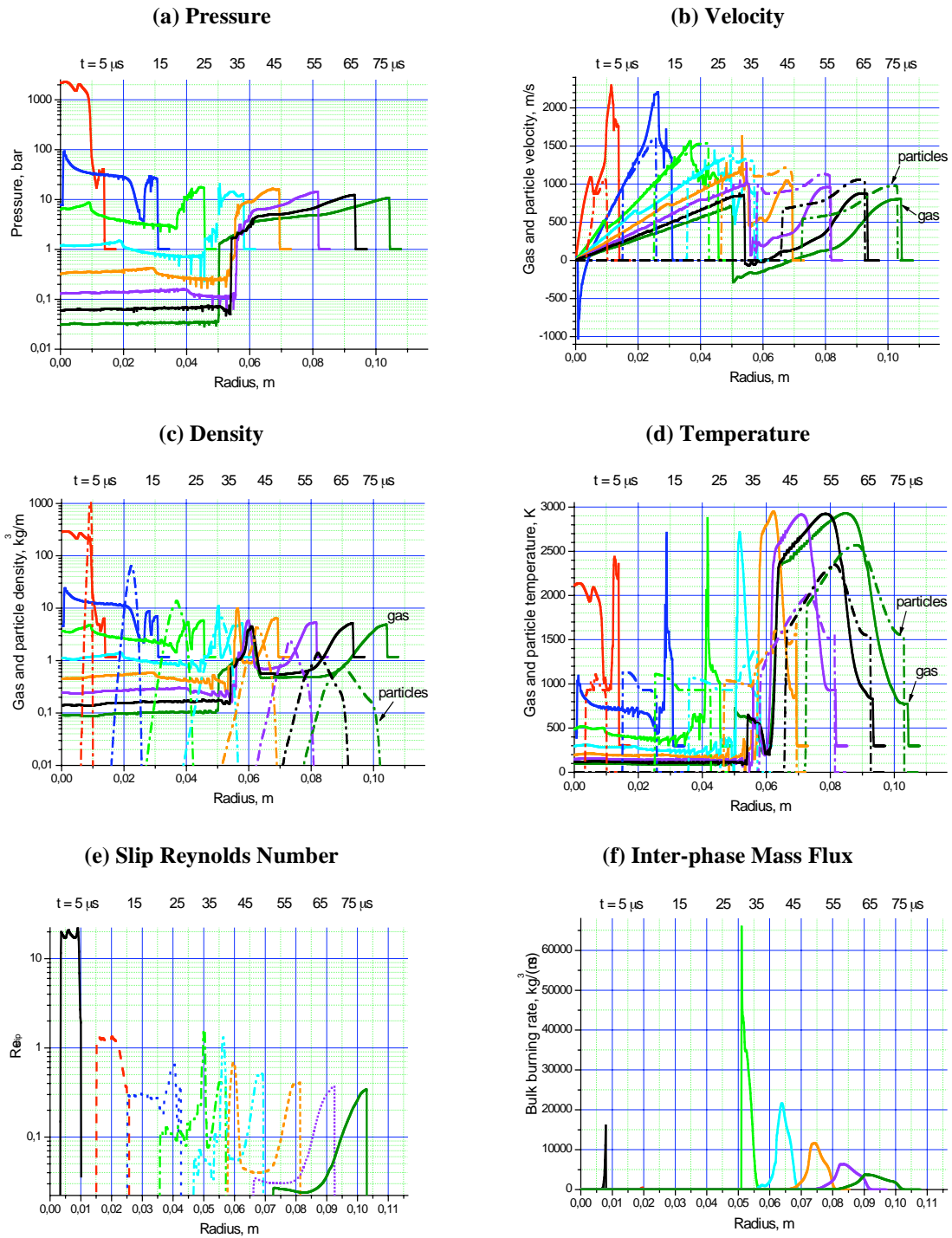


Figure 2. Two-phase blast wave profiles during the expansion phase of a 1.5-g Al-SDF explosion. Solid curves denote the gas phase and dashed curves indicate the particle phase.

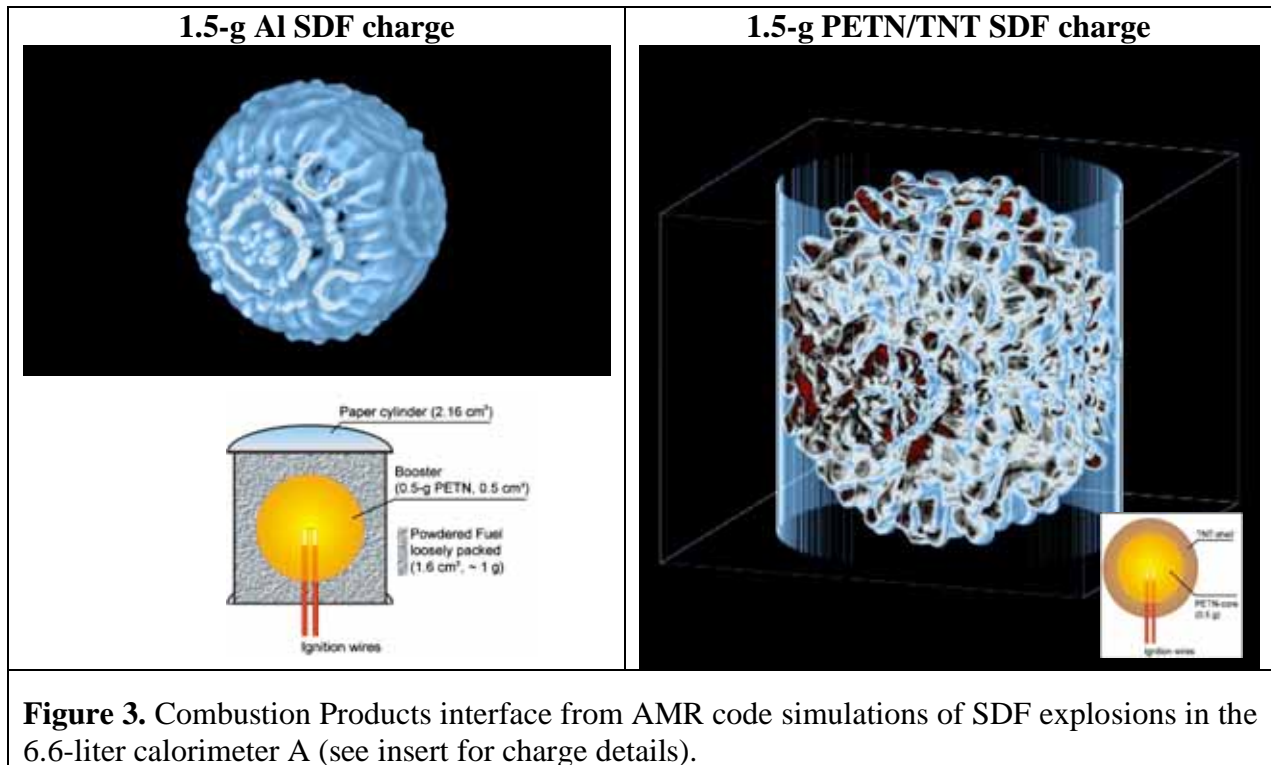


Figure 3. Combustion Products interface from AMR code simulations of SDF explosions in the 6.6-liter calorimeter A (see insert for charge details).

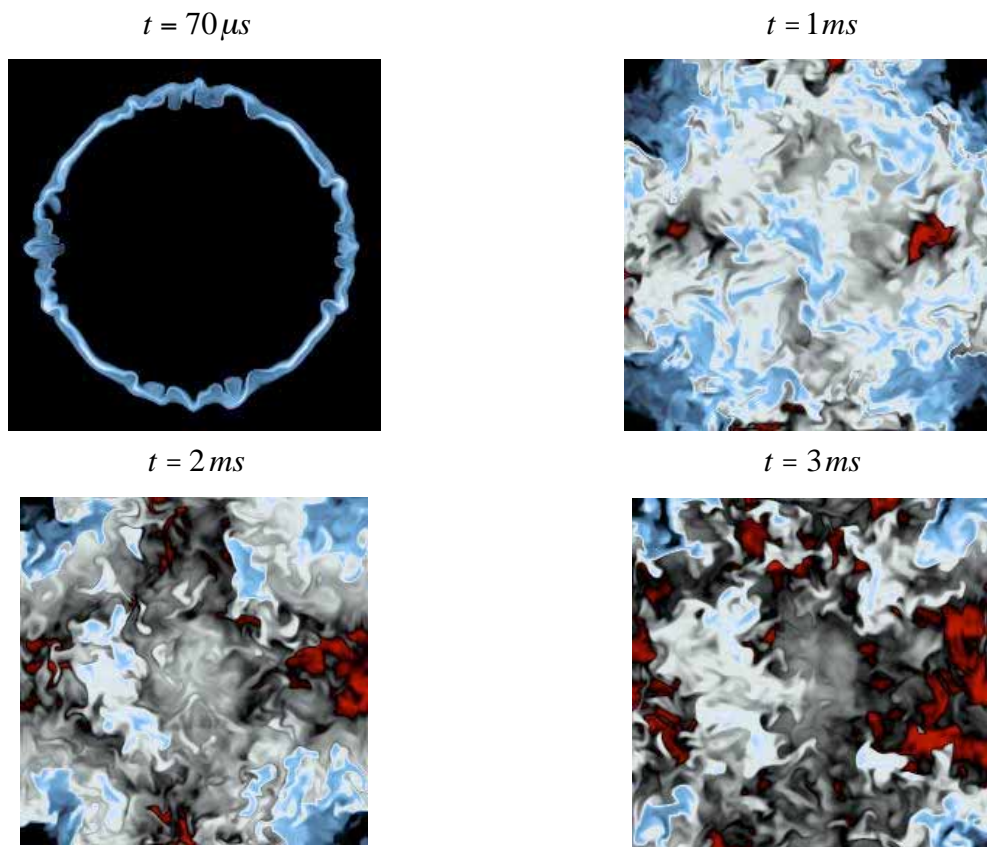


Figure 4. Cross-sectional views of the combustion Products concentration field in the mid-plane of the 6.4-liter cube at various times during the 3D AMR simulation (equilibrium model).

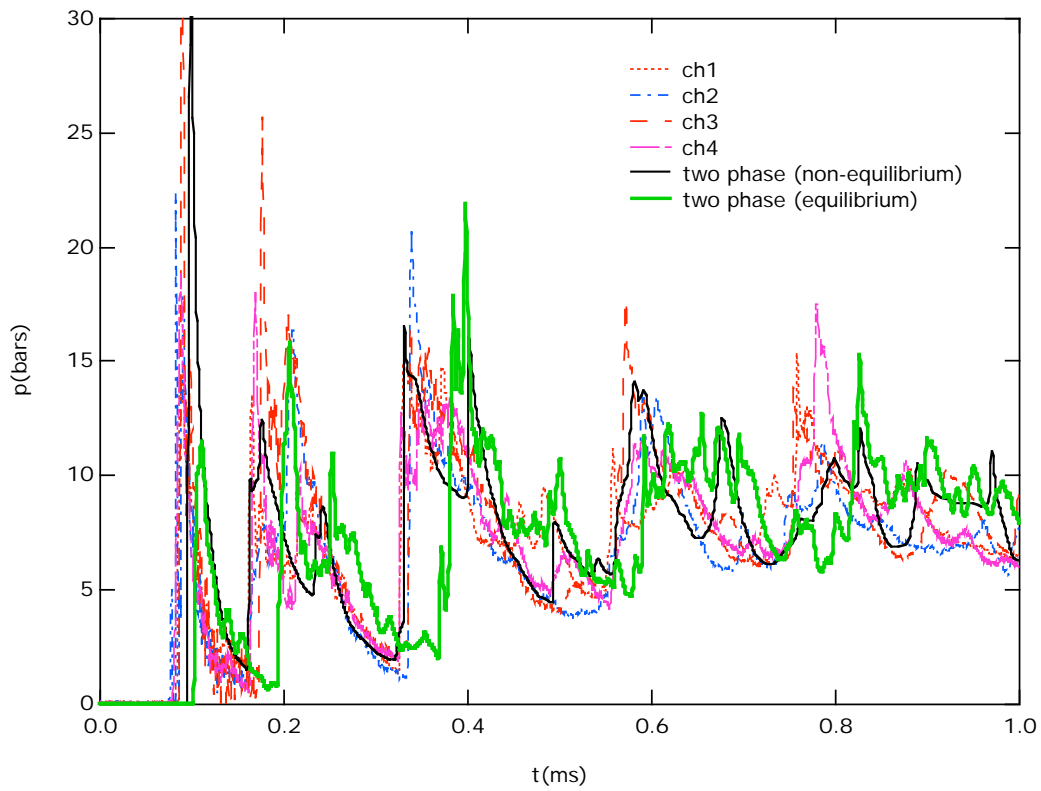


Figure 5. Pressure histories for the explosion of a 1.5-g Al-SDF charge in the 6.6-liter calorimeter (case A). Comparison of numerical simulations versus data.

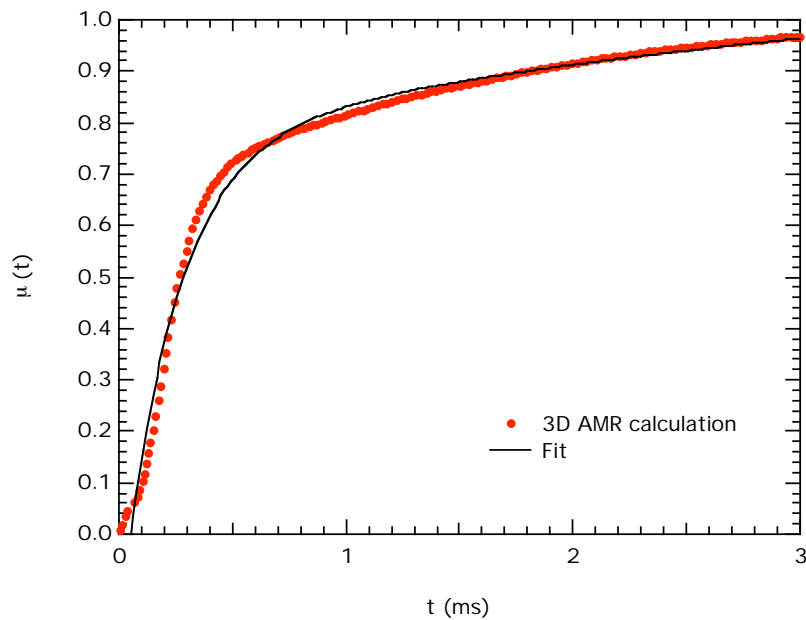


Figure 6. Mass fraction of fuel (Al) consumed from the 3D-AMR simulation. Results are fit by the Life function: $\mu(t) = 1.12 - 0.363e^{-0.284t} - 0.939e^{-4.20t}$.

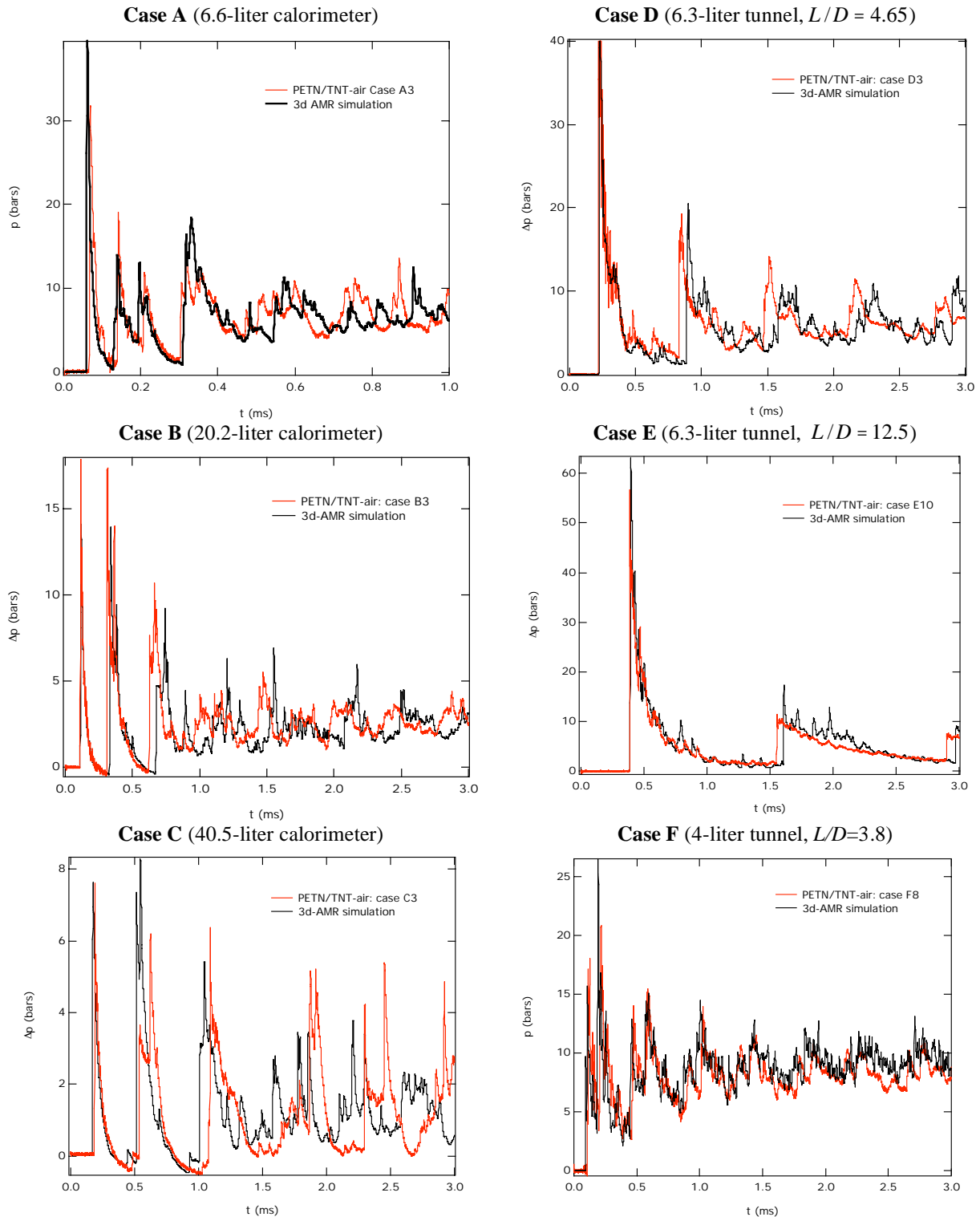


Figure 7. Comparison of pressure histories from numerical simulations with experimental data for explosion of 1.5-g PETN/TNT charges in cylindrical ($L/D=1$) chambers with different volumes (Cases A, B and C) and tunnels with different L/D ratios (Cases D, E and F).